frontiers | Frontiers in Earth Science

ORIGINAL RESEARCH
published: 08 June 2022
doi: 10.3389/feart.2022.885860

Geochemical Characteristics of Catalytic Hydrogenation of Low-Mature Kerogen Under Deep Fluids

Xiaowei Huang[1,2,3], *Zhijun Jin*[1,2,4]*, *Quanyou Liu*[1,2,4]*, *Qingqiang Meng*[2,4], *Dongya Zhu*[2,4], *Lu Wang*[1,2], *Jiayi Liu*[2,4], *Panpan Zhang*[2,3] and *Jingbin Wang*[2,3,4]

[1]Institute of Energy, Peking University, Beijing, China, [2]State Key Laboratory of Shale Oil and Gas Enrichment Mechanisms and Effective Development, SINOPEC, Beijing, China, [3]School of Energy Resources, China University of Geosciences (Beijing), Beijing, China, [4]Petroleum Exploration and Production Research Institute, SINOPEC, Beijing, China

There is increasingly valued attention on whether the matter and energy carried in the deep fluids can significantly change the hydrocarbon (HC) generation of low-mature source rocks. Previous studies suggest that the upward movement of deep fluids to sedimentary basins will change the HC generation evolution mode of low-mature source rocks, and the matter and energy carried by the fluid will transform the evolution process as transient events. However, there is a lack of quantitative evaluation of the specific changes of gaseous HC generation in the process of modification. In this study, the effect of deep fluids on HC generation and evolution of low maturity source rocks were quantitatively studied through simulation experiments of the gold tube closed system. We quantitatively selected hydrogen and catalysts ($ZnCl_2$ and MoS_2) to conduct catalytic hydrogenation of kerogen and explore the quantitative effects of deep fluids on HC generation in low-mature source rocks. Through the experimental results, it is found that catalytic hydrogenation has significant changes in a HC generation transformation of organic matter (OM). With the increase of catalytic hydrogenation reaction intensity, the maximum gaseous HC generation yield is 3.16–3.24 times that of the control groups without hydrogenation. In the relatively low-temperature stage (<400°C), the competitive hydrogenation effect occurs and the drying coefficient is high. After the high-temperature stage, a large amount of hydrogen participates in the reaction, which significantly promotes the increase of gaseous HCs and decreases the drying coefficient. $ZnCl_2$ or MoS_2 can change the relative content ratio of isomerism and isomorphism of butane and pentane, suggesting that cationic catalysis plays a greater role. In the reaction process, OM plays the most important role in the contribution to HC generation, exogenous hydrogen is more likely to participate in HC generation reaction than water and has the potential contribution to HC generation in Fischer-Tropsch synthesis (FFT) under catalytic conditions. The results of this study effectively verify that exogenous hydrogen and metal elements in deep fluids significantly modify the thermal evolution of low-mature source rocks, and enhance the HC generation potential in the high-temperature stage.

Keywords: simulation experiment, catalytic hydrogenation, gaseous yield, Xiamaling formation, FTT synthesis

OPEN ACCESS

Edited by:
Tongwei Zhang,
University of Texas at Austin,
United States

Reviewed by:
Dionysis Foustoukos,
Geophysical Laboratory (CIS),
United States
Shuai Yin,
Xi'an Shiyou University, China

***Correspondence:**
Zhijun Jin
jinzj1957@pku.edu.cn
Quanyou Liu
qyouliu@sohu.com

Specialty section:
This article was submitted to Geochemistry, a section of the journal Frontiers in Earth Science

Received: *28 February 2022*
Accepted: *23 May 2022*
Published: *08 June 2022*

Citation:
Huang X, Jin Z, Liu Q, Meng Q, Zhu D, Wang L, Liu J, Zhang P and Wang J (2022) Geochemical Characteristics of Catalytic Hydrogenation of Low-Mature Kerogen Under Deep Fluids. Front. Earth Sci. 10:885860. doi: 10.3389/feart.2022.885860

1 INTRODUCTION

The deep fluids carry a lot of matter and energy as the transport link between the interior and exterior of the sedimentary basin, which play a key role in the HC generation evolution of the young and low-mature HC source in the sedimentary basin has been paid much attention (Jin et al., 2002,2004; Meng et al., 2010; Liu et al., 2016, 2018). As one of the major components of deep fluids, hydrogen is widely distributed in geological strata (Sherwood-Lollar et al., 2014; Meng et al., 2015; Etiope, 2017; Guelard et al., 2017; Etiope and Whiticar, 2019; Bougault et al., 2019; Klein et al., 2019; Klein et al., 2020). Meanwhile, there are lots of metal elements in the deep fluids (e.g., Mg, Fe, Mn, Zn, and Mo) (Tivey, 2007; Resing et al., 2015).

For the study on HC promotion by adding H_2, Jin et al. (2004) found that deep hydrogen-rich fluids can promote HC generation of source rocks. Meng et al. (2015) confirmed that deep hydrogen-rich fluids can activate and increase the HC regeneration of ancient source rocks. Liu et al. (2016) found deep fluids can make a contribution to inorganic methane by Fischer-Tropsch synthesis in Songliao Basin, China. Huang et al. (2021) verified that H_2 plays a dominant role in the contribution of sufficient deep hydrogen-rich fluid to the HC promotion of high-mature kerogen. Meanwhile, the effects of transition metals on HC generation of OM have been widely studied (Mango, 1996; Mango and Hightower, 1997; Medina et al., 2000; Lewan et al., 2008; He et al., 2011; Ma et al., 2018). Transition metals can significantly promote the decomposition of OM and generate methane-rich gas, and the content of gas products was similar to the composition of natural gas through simulation experiments with the addition of transition metal Ni or NiO, and the transition metal elements play a major role in natural gas generation through catalytic action (Mango, 1996; Mango and Hightower, 1997). He et al. (2011) analyzed the catalytic mechanism of MoS_2 in two aspects through a simulation control experiment: the generation of H_2S through MoS_2 reduction can trigger the free radical reaction of HCs, and the Lewis acid site provided by the transition metal Mo can promote the homolysis of H_2 to generate H free radical, and promote the catalytic HC generation of OM. Ma et al. (2018) showed that pyrite plays a catalytic role by converting into pyrrhotite and monovalent sulfur, which can reduce the isomerization degree and promote the generation of saturated HCs. However, previous studies have not determined the synergistic reaction and quantitative transformation evaluation of hydrogen and catalysts in catalytic hydrogenation reaction of low-mature source rocks. In the simulation experimental study of catalytic hydrogenation of low mature HC source rocks, it is difficult to accurately quantify the gaseous reactant hydrogen, and there are few quantitative studies on the comparison of reaction participation degree, which makes it difficult to accurately quantify and evaluate the contribution of hydrogen to HC generation.

Therefore, the effects of external hydrogen sources and catalysts on HC generation of low-mature source rocks were investigated with the gold tube closed system experimental reaction system. It was believed that HC generation transformation of low-mature source rocks by deep fluids was an "instantaneous event" in geological history, catalytic hydrogenation effects on the yield of gaseous products confirmed further potential of HC generation in low-maturity marine I-type kerogen in the quantitative hydrogenation process.

2 EXPERIMENTAL SAMPLES AND METHODS

2.1 Experimental Samples

The low-maturity source rock samples selected in the experiment were taken from the bottom of the Middle Proterozoic Xiamaling Formation (Fm.) in the Xiahuayuan section in Northern China. The lithologic character is argillaceous limestone with strong HC generation capacity, low thermal maturity and retain abundant early HC generation parent materials (Sun et al., 2003; Zhang et al., 2007; Xie et al., 2013; Guo et al., 2014). The rock samples were washed with deionized water to remove surface impurities, then left to dry in a fume hood and ground to 200 mesh powder particles using a grinder. The mixed solvent of CH_2Cl_2 and HCOOH with a volume ratio of 9:1 was used to extract the rock samples for 72 h by the soxhlet extraction method. After that, the extracted powder was treated with HCl acid at a constant temperature of 80°C for 8 h to remove carbonate minerals, and then the remaining powder was washed with deionized water to pH = 7.0 to remove HCl acid. Then the powder was treated with the mixed solution of HCl and HF with a 1:1 volume ratio for 8 h, and acid treatment was performed to remove the excess inorganic minerals. After that, the powder was washed with deionized water to pH = 7.0 and dried in a fume cabinet to evaporate the excess water to finish kerogen preparation.

The catalyst $ZnCl_2$ powder is produced by Aladdin Reagent Company with a purity of 99.95%. MoS_2 powder is produced by Aldrich Chemical Reagent Company with a purity of 99.00%. The particle sizes of the two reagents were both 200 mesh, which reached the purity standard of experimental analysis. Deionized water was prepared in the laboratory. H_2 was stored in the gas cylinder with 5% molar volume He as the internal standard gas.

The basic geochemical data of the prepared kerogen samples were analyzed, Rock-eval and Vitrinite reflectance Ro parameters were tested to determine the content of HC and other elements in OM and the amount of reactants in a quantitative experiment. The kerogen is type I, and the thermal maturity (Ro) is 0.63%. The total organic carbon (TOC) content is 88.0% with purification. Tmax is 433°C, and pyrolysis parameter S1 is 2.22 mgHC/g ker. S2 = 342.12 mgHC/g ker, S3 = 34.74 mg HC/g ker, hydrogen index (HI) = 389, oxygen index (OI) = 39, which are typical low evolution hydrogen-rich kerogen.

2.2 Experimental Method

The experimental work was carried out in the State Key Laboratory of Organic Geochemistry, Guangzhou Institute of Geochemistry, Chinese Academy of Sciences. Sample loading involves quantitative loading of solid, liquid, and gaseous three-phase samples. For the quantitative loading steps of solid and liquid samples in the control group with H2 addition, specific

experimental methods of predecessors were mainly referred to (Liu and Tang, 1998; Huang et al., 2021). The reactants were 24.00 mg kerogen powder, 24.00 mg deionized water, 2.40 mg catalyst powder, and 0.60 mg H2. After completing the above sample loading, the gold tubes are placed into the high-temperature reactor and heated. The heating program is set to reach each predetermined temperature point in 2 h and then heated for 72 h. There are four experimental samples of different control groups with each set at six temperature points, 300°C, 350°C, 375°C, 400°C, 450°C, 500°C, and 550°C. The pressure in the simulation experiment was set at 500bar, and the abnormal pressure change in the heating reactor was controlled within ±1bar. Experimental group IA is kerogen + deionized water + $ZnCl_2$; group IIA is kerogen + deionized water + MoS_2; group IIIA is kerogen + deionized water + $ZnCl_2$+H_2; group IVA is kerogen + deionized water + MoS_2+H_2.

The gold tubes were removed from the reactor and cleaned after heating, then the gold tube was slowly placed into a custom-made vacuum glass tube connected to the Agilent 6890N full-component gas chromatography (GC) modified by Wasson ECE Instrumentation company from the US. The GC consists of two TCD detectors and one FID detector. The detection column is a Paraplot Q capillary column (25 m × 0.32 mm × 10 μm). The heating procedure was to set at the initial temperature at 50°C for 3 min, then raised to 190°C at a rate of 25°C/min and kept for 5 min (Wang et al., 2020; Huang et al., 2021).

3 RESULTS

The simulation experiment results show that the total yield of gas components in all groups has a rising trend with increasing temperature. The detected organic components were divided into $C_{1\sim5}$, and the inorganic components were divided into CO_2 and H_2. The total gas production rate of group IA starts from 46.78 m^3/t at the initial temperature of 300°C and reaches the maximum yield of 561.99 m^3/t at the maximum temperature of 550°C. The total gas production rate of group IIA starts from 46.19 m^3/t at the initial temperature of 300°C, and the maximum gas yield was 441.75 m^3/t at 550°C. Between 300 and 375°C, the total gas yield under the action of MoS_2 was slightly higher than that under the action of $ZnCl_2$. After 400°C, the total gas yield under the action of $ZnCl_2$ was significantly higher than that under the action of MoS_2. In groups IIIA and IVA, the total gas yield (H_2 yield not calculated) was 44.36 m^3/t and 29.87 m^3/t at 300°C, respectively. The yield increased significantly with the temperature increase. At 550°C, the maximum yields are 1,283.85 m^3/t and 1,064.92 m^3/t, which are 2.3 and 2.4 times of the maximum yields of IA and IIA groups without H_2 groups, respectively. Moreover, the effect of $ZnCl_2$ on the increase of total gas yield is greater than that of MoS_2. Compared with groups IA and IIA, the CO_2 yield of the control group was significantly reduced after adding the H_2 reaction. The alkane yield shows a decreasing trend at 300–400°C and is mainly inhibited at a low temperature. After 450°C, the alkane yield increases greatly. Alkanes yield is significantly affected by temperature change, while CO_2 yield is insignificant at 300°C–450°C and significant at a higher temperature.

The total gaseous HC yield distribution of $\sum C_{1\text{-}5}$ increased from the initial low-temperature to the high-temperature stage and reached the maximum at 550°C. The initial temperature yield of total gaseous HCs in group IA is 1.52 m^3/t and the maximum yield is 366.67 m^3/t. The initial temperature yield of total gaseous HCs in group IIA is 2.73 m^3/t and the maximum yield is 298.13 m^3/t. The maximum yield of total gaseous HCs in groups IA and IIA increases steadily with the temperature increase. The initial temperature yield of total gaseous HCs in group IIIA is 9.91 m^3/t, and the maximum yield is 1,158.59 m^3/t. The initial yield of total gaseous HCs in group IVA is 7.67 m^3/t, and the maximum yield is 966.60 m^3/t. The maximum yield of $\sum C_{1\text{-}5}$ increases with the increase of temperature in IIIA and IVA groups. The maximum yields of hydrogenated groups IIIA and IVA are 3.16 and 3.24 times that of groups IA and IIA without H_2, respectively (**Figure 1A**).

The distribution of C_1 changes from low temperature to high temperature, and the total gaseous HC yield increases continuously (**Figure 1B**), reaching its maximum value at 550°C. The initial temperature yield of total gaseous HCs in group IA is 1.06 m^3/t and the maximum yield is 365.34 m^3/t. The initial temperature yield of total gaseous HCs in experimental group IIA is 1.94 m^3/t and the maximum yield is 294.27 m^3/t. The maximum yield C_1 in groups IA and IIA increases relatively gently with the increase of temperature. The initial temperature yield of total gaseous HCs in group IIIA was 7.07 m^3/t, and increase with the increase of temperature, the maximum yield was 1,029.01 m^3/t. The initial temperature yield of total gaseous HCs in group IVA was 5.72 m^3/t, and the maximum yield was 938.48 m^3/t. And the yield of total gaseous HCs was increased with the increase of temperature. In groups IIIA and IVA, the maximum yield C_1 increased significantly with the increasing temperature. The maximum yield of hydrogenated groups IIIA and IVA are 2.82 and 3.19 times that of groups IA and IIA without H_2.

In terms of the distribution of C_2 yield (**Figure 1C**), the C_2 yield of IA and IIA groups increased from the initial temperature of 300°C–450°C, respectively, and reached the maximum yield at 450°C, which decreased from 450 °C to 550°C. The maximum yield of C_2 was 59.79 m^3/t (450°C) and 61.05 m^3/t (450°C), respectively. There was no significant difference in the temperature change curve of C_2 yield under $ZnCl_2$ and MoS_2. The maximum yields of C_2 in IIIA and IVA groups were 378.73 m_3/t (500°C) and 283.01 m^3/t (500°C), which were 6.33 and 4.64 times higher than those in IA and IIA groups with only catalyst, respectively. During the reaction process, the addition of exogenous H_2 inhibited the increase of C_2 yield in the range of about 300°C–410°C, and the ethane yield increased rapidly with the temperature rising from about 410°C. The participation of H_2 in the reaction at high temperature delayed the peak temperature point of C_2 HC generation, and the increase of C_2 yield under $ZnCl_2$ was larger than MoS_2.

The C_3 yields of IA and IIA groups showed an overall increasing trend from the initial temperature of 300°C–450°C, respectively, and reached the maximum yield between 400°C and 450°C, after which the yield decreased with the increase of temperature. The maximum C_3 yields were 14.84 m^3/t (400°C)

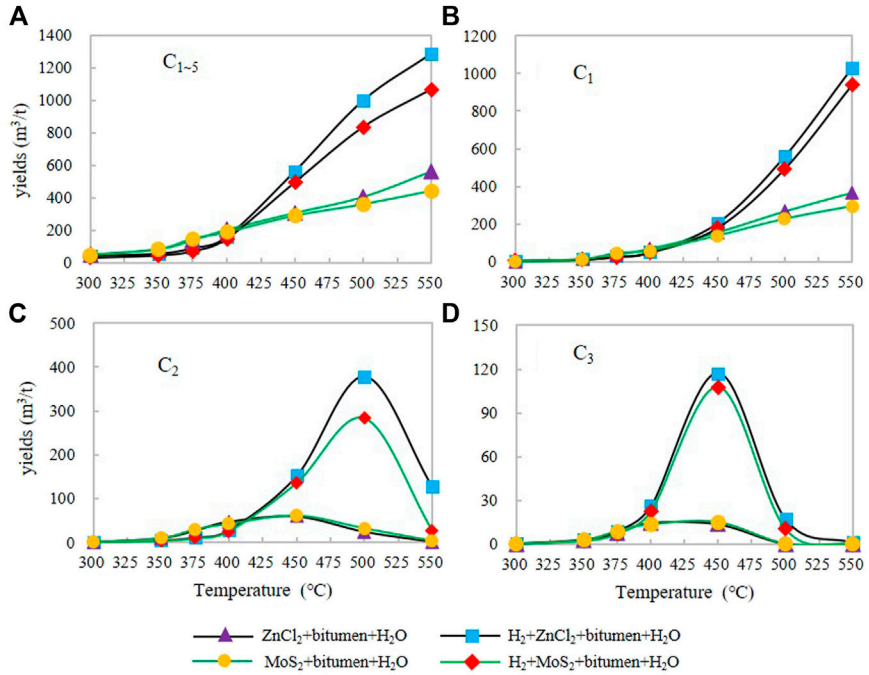

FIGURE 1 | The yield characteristics of $C_{1\sim5}$**(A)**, C_1**(B)**, C_2**(C)**, C_3**(D)** under different catalytic hydrogenation control conditions of the closed system.

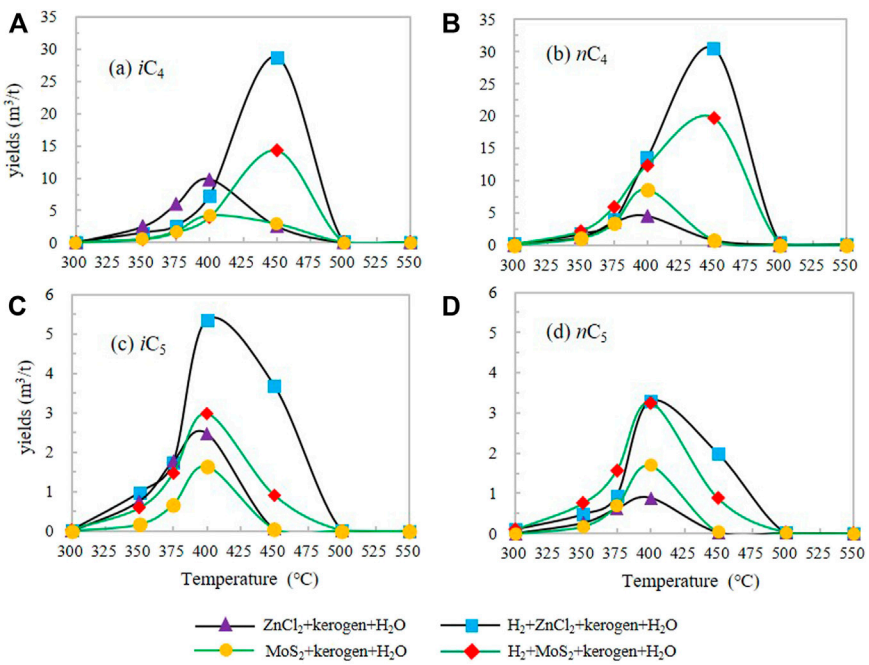

FIGURE 2 | The yield characteristics of iC_4**(A)**, nC_4**(B)**, iC_5**(C)**, nC_5**(D)** under different catalytic hydrogenation control conditions of the closed system.

and 14.95 m^3/t (450°C), respectively. In groups IIIA and IVA, the maximum C_3 yields were 117.16 m^3/t (500°C) and 107.55 m^3/t (500°C), respectively (**Figure 1D**), which were 7.89 and 7.19 times higher than those of the IA and IIA groups without H_2 addition, respectively. The addition of exogenous H_2 inhibited the increase of C_3 yield from 300°C to 375°C and increased significantly after 400°C. The participation of H_2 in the reaction at high temperature delayed the peak temperature of C_3 HC generation, and the

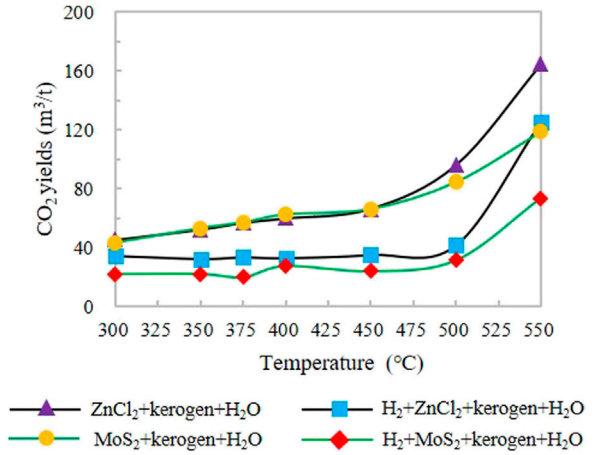

FIGURE 3 | Change in CO_2 yield simulated under different catalytic hydrogenation control conditions of the closed system.

increase of C_3 yield under $ZnCl_2$ was greater than that under MoS_2. The addition of exogenous H_2 inhibited the growth of C_3 yield from 300°C to 375°C and significantly increased C_3 yield after 400°C.

The change of iC_4 yield in IA and IIA groups increased from the initial temperature first, reaching the maximum yield of 3.62 m^3/t and 1.67 m^3/t at 400°C, respectively, and then decreased rapidly with the increase of temperature. The maximum yield of iC_4 in IIIA and IVA groups was 25.04 m^3/t (450°C) and 11.99 m^3/t (450°C), respectively, which were 6.92 and 7.18 times of the maximum yield in I and II groups without H_2 (**Figure 2A**).

The nC_4 yield in groups IA and IIA increased from the initial temperature and reached the maximum yield at 400°C, and then decreased with the increase of temperature. The maximum yield of nC_4 was 3.85 m^3/t (400°C) and 4.29 m^3/t (400°C), respectively. After the H_2 reaction was added in groups IIIA and IVA, the maximum yield of nC_4 was 22.75 m^3/t (450°C) and 23.71 m^3/t (450°C) (**Figure 2B**), which are 5.91 and 5.53 times of that in groups IA and IIA without H_2, respectively. The addition of exogenous H_2 delayed the peak of HC generation of i/nC_4 to the high-temperature point and significantly increased the yield of iC_4 and nC_4, among which, the effect of promoting the yield of nC_4 was greater than that of iC_4.

The variation of iC_5 yield of groups IA and IIA increased from the initial temperature first, and reached the maximum yield in the range of 400°C–450°C. After that, the yield decreased with the increase of temperature. Maximum yields of iC_5 were 0.69 m^3/t (400°C) and 0.81 m^3/t (400°C), respectively. The maximum yields of iC_5 in groups IIIA and IVA were 3.22 m^3/t (400°C) and 2.43 m^3/t (400°C), respectively, which were 4.67 and 3.00 times higher than those in IA and IIA groups without H_2 addition, respectively.

For n-pentane nC_5 (**Figure 2D**), nC_5 production in groups IA and IIA firstly increased from the initial temperature of 300°C, and reached the maximum yield of 0.36 m^3/t and 0.97 m^3/t at 400°C, respectively. After that, the yield decreased rapidly with the increase of temperature. The maximum yield of nC_5 was 2.82 m^3/t (450°C) and 4.33 m^3/t (450°C) in groups IIIA and IVA after H_2 reaction, which was 7.83 and 4.46 times of that in groups IA and IIA, respectively. The addition of exogenous H_2 significantly promoted the increase of HC generation yield of i/nC_5 and delayed the peak temperature of HC generation of i/nC_5. Among them, the HC increasing effect of nC_5 is greater than that of iC_5.

CO_2 production increases continuously from the initial temperature to the high-temperature stage, and reaches its maximum value at 550°C. The minimum CO_2 yield in groups IA and IIA was 45.21 m^3/t (300°C) and 43.44 m^3/t (300°C), and the maximum CO_2 yield was 164.65 and 119.02 m^3/t (550°C), respectively (**Figure 3**). The minimum CO_2 yields of groups IIIA and IVA were 34.47 m^3/t (350°C) and 22.18 m^3/t (350°C), which were 0.76 and 0.51 times of the minimum CO_2 yields of IA and IIA groups without H_2 addition, respectively. The maximum CO_2 yields were 125.30 m^3/t and 73.72 m^3/t, respectively, which were 0.76 and 0.62 times higher than those of IA and IIA without H_2. The comparison of the experimental results shows that the addition of H_2 leads to a significant decrease in CO_2 yield, and the CO_2 yield remains stable with the change of temperature between 300°C and 550°C.

H_2 production distribution of gaseous products in groups IA and IIA increased continuously from low temperature to high temperature, reaching the maximum at 550°C (**Figure 4**). The maximum H_2 production of groups IA and IIA were 30.67 m^3/t and 24.60 m^3/t, respectively. The results show that H_2 generation is significantly promoted by the addition of catalyst. Compared with MoS_2, $ZnCl_2$ has a greater effect on H_2 yield, with an average of 1.2 times. Combined with the study on the catalytic hydrogenation of highly mature kerogen (Huang et al., 2021), the main H element of H_2 generation comes from OM itself. The H_2 yields of groups IIIA and IVA are the amount of consumption involved in the reaction. All the H_2 yield changes show one positive linear relationship between ln (H_2) and temperature.

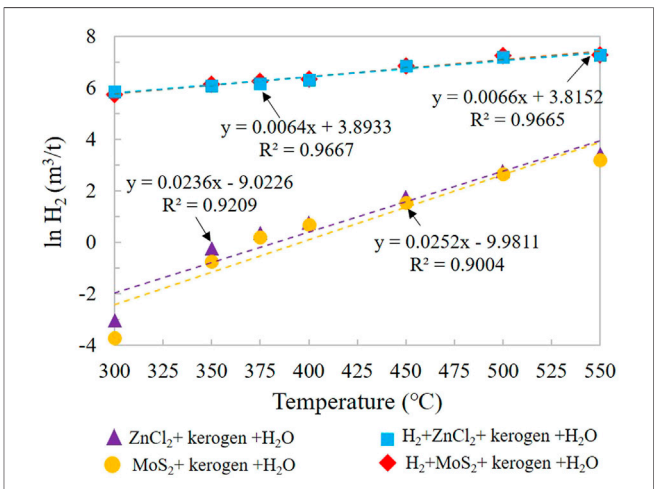

FIGURE 4 | Change in H_2 yield simulated under different catalytic hydrogenation control conditions of the closed system.

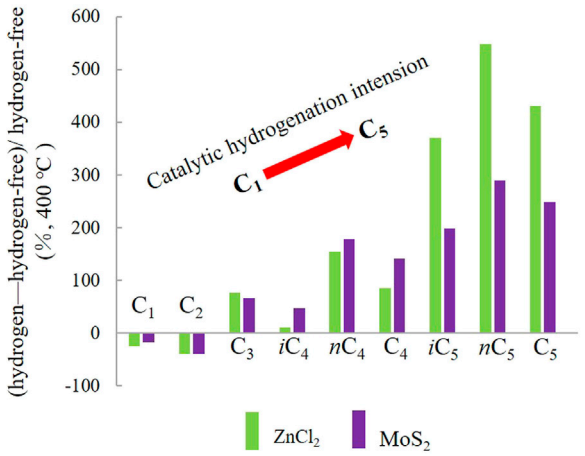

FIGURE 5 | Comparison of C_{1-5} production under $ZnCl_2$ and MoS_2 at 400 °C in closed system.

4 DISCUSSION

4.1 H_2 Contribution on Gaseous HC Generation

4.1.1 HC Generation Promotion

During the low-temperature stage (300°C–400°C), the gaseous HC yields of the H_2 groups are lower than those of the H_2-free groups under the catalysis for the low-mature kerogen. For example, the results at 400°C (**Figure 5**) show that, under the action of $ZnCl_2$ and MoS_2, the C_1 yields after the H_2 reaction increased by 17.49 m^3/t and 9.57 m^3/t, respectively, accounting for 25.0% and 16.6% of the C_1 yield of the groups without H_2, respectively. C_2 yields increased by 19.03 m^3/t and 16.52 m^3/t, accounting for 39.8% and 38.9% of those with H_2-free groups, respectively. The C_3 yield increased by 11.45 m^3/t and 9.12 m^3/t, accounting for 77.2% and 67.0% of C_3 yield without the H_2 groups, respectively. The yield variation of C_4 and C_5 was similar to that of C_3. Compared with C_3, the yield increased more after exogenous H_2 was involved in the reaction. This is due to the joint determination of the bond energy of the macromolecular groups of kerogen and the activation energy provided by the outside. As the bond energy of different HC groups in kerogen decreases with the increase of C number, the reaction is less affected by the external energy and catalytic action at the relatively low-temperature stage, which leads to preferential fracture of long-chain alkyl groups to generate shorter HCs (Dai, 2014). At the same time, under the condition of mass conservation of total active carbon, the content of active C involved in the synthesis of small molecules such as C_1, C_2, and C_3 decreased, resulting in a significant decrease in the yield of gaseous light HCs compared with adding H_2 groups. Therefore, HC generation at low-temperature is mainly controlled by pyrolysis of organic components of low-mature kerogen. In high-temperature phase, the kerogen is affected by external energy and catalytic increases gradually, under the effect of catalyst and H_2, the gaseous HC production rate increases significantly, and increase of CH_4 as the most stable HC molecule, its yield increase composite generated by kerogen cracking itself and other C_{2+} hydrogenation cracking from the combined impact of the contrast experiment under the same condition of, the methane yield under $ZnCl_2$ is higher than MoS_2. For C_{2+} gaseous HCs, the bond energy of gaseous HC groups decreases with the increasing carbon number (e.g., -C_5<-C_4<-C_3<-C_2), which promote the C_{2+} groups to react with H_2 preferentially, resulting in the significant increasing yields of the C_{2+} HCs.

4.1.2 Drying Coefficient

The catalytic hydrogenation takes prominent effects on the drying coefficient ($C_1/\sum C_{1-5}$). All the experimental group values of $C_1/\sum C_{1-5}$ showed a trend of decreasing, and then increasing with higher temperatures (**Figure 6**). In IA and IIA groups, $C_1/\sum C_{1-5}$ decreased firstly and then increased from low temperature to high temperature, $C_1/\sum C_{1-5}$ decreased from initial temperature (300°C) about 0.70 and 0.71 to the minimum temperature 0.50 (350°C) and 0.47 (350°C), respectively, and $C_1/\sum C_{1-5}$ increased from 350°C to 375°C. After 400°C, $C_1/\sum C_{1-5}$ values increase continuously under the participation of $ZnCl_2$ and MoS_2 and reach the maximum $C_1/\sum C_{1-5}$ values of 1.00 and 0.99 at 550°C. $C_1/\sum C_{1-5}$ was more significant than $ZnCl_2$ under MoS_2 catalysis.

The $C_1/\sum C_{1-5}$ of groups IIIA and IVA, in which exogenous H_2 and catalyst were involved in the reaction together, firstly decreased and then increased from the initial low temperature to the high-temperature stage, continuously decreased from 0.71 to 0.75, respectively, and decreased to the minimum value of 0.39 and 0.38 at 450°C, respectively. The continuous increase of C_1 produced by catalytic hydrocracking of kerogen or C_{2+} component and the decrease of C_{2+} component yield resulted in a rapid increase of $C_1/\sum C_{1-5}$, reaching the maximum values of 0.89 and 0.97 at 550°C, respectively.

The $C_1/\sum C_{1-5}$ values of the XML Fm. with H_2 increased from 300 to 375°C, while the $C_1/\sum C_{1-5}$ values of the Yurtus Fm. with H_2 decreased (Huang et al., 2021). It indicates that this is caused by

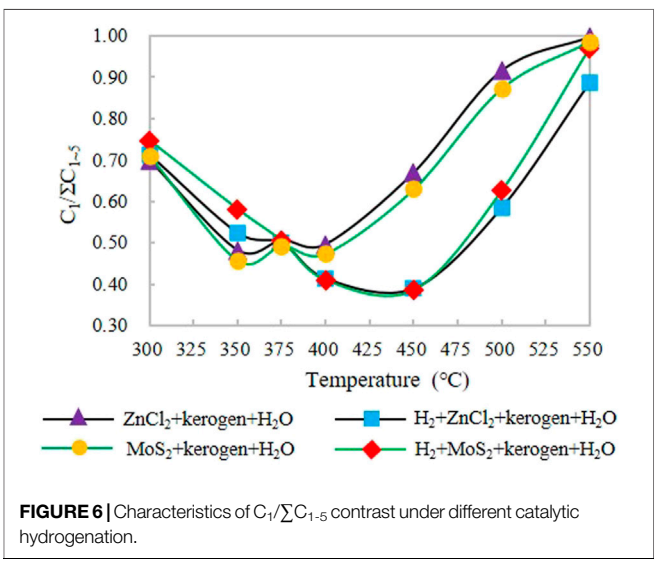

FIGURE 6 | Characteristics of $C_1/\sum C_{1-5}$ contrast under different catalytic hydrogenation.

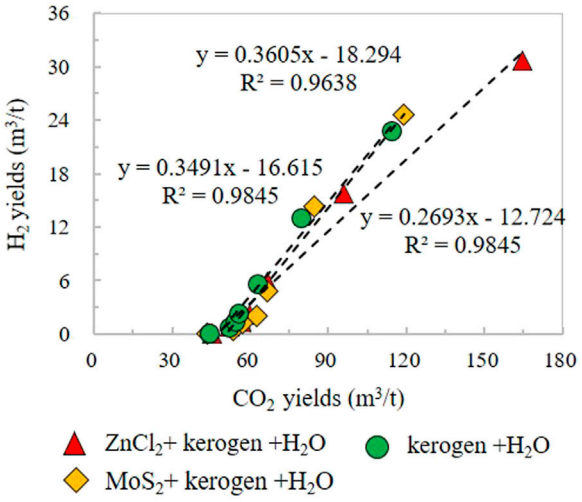

FIGURE 7 | Correlation changes of the synergistic yields between H_2 and CO_2.

the structural differences between the two kerogens. Both Xiamaling Fm. and Yurtus Fm. develop Marine type I kerogens in ancient layers, while Xiamaling Fm. is low-mature kerogens with aliphatic branch chains and heteroatomic groups (Sun et al., 2003; Guo et al., 2014). At the same time, the gaseous HC production rate also decreased after the H_2 addition reaction, which was speculated to be due to the binding reaction of exogenous H_2 with the upper branch chain of low-mature kerogen molecule or other heteroatomic groups, which inhibited the generation of gaseous HC. After 375°C, hydrogenation increases the gaseous HC yield more significantly, promotes the generation of C_{2+}, and increases the temperature point at which $C_1/\sum C_{1\text{-}5}$ reaches the minimum value, which is mainly due to the early generation of the addition reaction of exogenous H_2. Furthermore, the drying coefficient of the product decreased significantly, and the temperature of the minimum drying coefficient was delayed relative to that of the H_2 groups.

4.2 Contribution of Different Hydrogen Sources to HC Generation

In the simulated reaction experiment of kerogen with only water or catalyst in Xiamaling Fm., there was a good linear positive correlation between CO_2 and H_2 yields, H_2 (catalyst free) = 0.3491CO_2-16.615, R^2 = 0.9845. H_2 (MoS_2) CO_2 = 0.3605 18.294, R^2 = 0.9638; H_2 ($ZnCl_2$) = 0.2693CO_2-12.724, R^2 = 0.9845 (**Figure 7**). The above results indicate that H element in the H_2 and the C element in CO_2 are homologous, and both come from OM itself. Compared with the reaction change equation of the Yurtus Fm., the slope is larger, and the intercept value of the horizontal axis is significantly smaller than that of the Yurtus Fm., which indicating the low-mature kerogen has stronger pyrolysis capacity than that of high-mature kerogen. Under the same temperature and pressure conditions, the low-mature Xiamaling kerogen is more likely to generate more H_2.

By comparing the yield changes of lnH_2 and temperature of the Xiamaling Fm. under the action of catalyst, it was found that lnH_2 = 0.0252T-9.9811, R^2 = 0.9004 under the action of MoS_2; lnH_2 = 0.0236T-9.0226, R^2 = 0.9209 under $ZnCl_2$ catalysis. Temperature (T) and lnH_2 under the each catalyst showed good positive correlation linear characteristics and high fitting degree (**Figure 4**). Although the amount of H_2 produced by the low-mature kerogen of Xiamaling Fm. is larger than that of the high-mature kerogen of Yurtus Fm., the contribution of $ZnCl_2$ or MoS_2 to the catalytic action of Xiamaling Fm. is relatively smaller, and the difference of $ZnCl_2$ and MoS_2 in the catalytic effect of Xiamaling Fm. kerogen is also significantly smaller than that of Yurtus kerogen. It is speculated that the molecular structure of kerogen at the low-mature stage is more developed than that of alkane at the high-mature stage, and the bond energy is smaller. Therefore, the activation energy reduced by external catalysis has relatively little influence on H_2 generation from pyrolysis. In addition, in the adding H_2 groups, the linear relationship between lnH_2 and T under MoS_2 catalysis is lnH_2 = 0.0066T + 3.8152, R^2 = 0.9665. The linear relationship between lnH_2 and T under $ZnCl_2$ catalysis is lnH_2 = 0.0064T + 3.8933, R^2 = 0.9667, both of which also have a good linear relationship. At the initial temperature of 300°C, the minimum consumption of exogenous H_2 is 457.81 m^3/t, which is more easily involved in the catalytic hydrocracking reaction of Kerogen in the Xiamaling Fm. than H_2O. However, the actual participation amount of H_2 in this series of reactions was significantly smaller than that of high-mature kerogen, suggesting that the molecular structure of Kerogen in The Yurtus Fm. was higher in aromatization and contained lower HI abundance, leading to the need for more exogenous hydrogen to participate in the catalytic cracking reaction.

Therefore, the difference in consumption of hydrogen generation and H_2 participation in catalytic pyrolysis of kerogen with different maturity, as well as the lower yield of $C_{1\sim4}$ in the initial low-temperature stage of catalytic H_2 addition reaction in the Xiamaling Fm. than that in the reaction without H_2 addition, indicated that H element in Xiamaling kerogen itself would participate in the reaction prior to external H_2.

4.3 Different Effects Under Catalytic Hydrogenation

4.3.1 i/n Ratio Changes

As for the comparison of C_4 and C_5 in the Xiamaling Fm., the comparison of iC_4/nC_4 and iC_5/nC_5 at the same temperature showed that the i/n under the catalytic action of $ZnCl_2$ is larger than that under the action of MoS_2, and the ratio was significantly reduced with the H_2 reaction. The iC_4/nC_4 ratios of the products formed only under $ZnCl_2$ or MoS_2 catalysts from the initial temperature are 0.63–2.10 (N = 6, Ave. = 1.13) and 0.35–1.84 (N = 6, Ave. = 0.76), respectively (**Figure 8A**). The average ratio of iC_4/nC_4 in $ZnCl_2$ is about 1.49 times that in MoS_2, indicating that Zn^{2+} catalyzes iC_4 more strongly than Mo^{2+} and S^{2-}. In the adding H_2 groups, the iC_4/nC_4 ratios of $ZnCl_2$ and MoS_2 are 0.39–1.10 (N = 6, Ave. = 0.57) and 0.03–0.51 (N = 6, Ave. = 0.26),

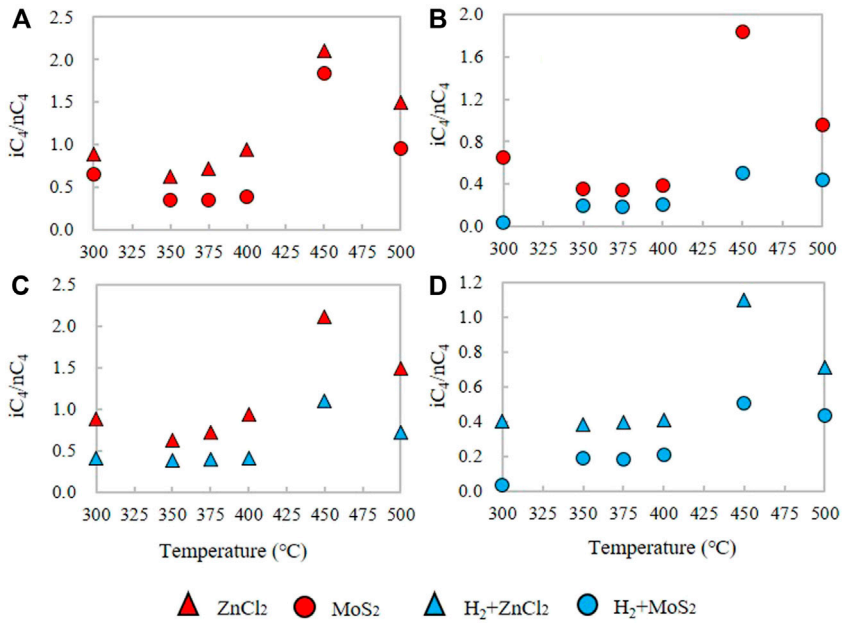

FIGURE 8 | Comparison of the iC_4/nC_4 alkane ratio under the $ZnCl_2$, MoS_2, H_2+$ZnCl_2$, and H_2+MoS_2 conditions for the kerogen in closed system.

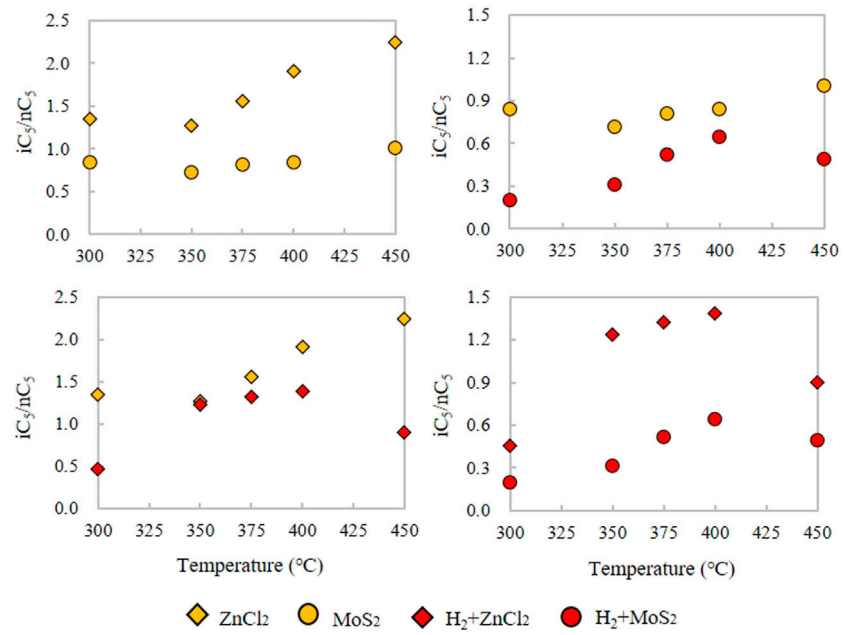

FIGURE 9 | Comparison of the iC_5/nC_5 alkane ratio under the $ZnCl_2$, MoS_2, H_2+$ZnCl_2$, and H_2+MoS_2 conditions for the kerogen in closed system.

respectively (**Figure 8D**). The iC_4/nC_4 values under $ZnCl_2$ were about 2.19 times higher than those under MoS_2. At the same time, the H_2 groups under $ZnCl_2$ and MoS_2 are 0.34 and 0.31 of the iC_4/nC_4 ratio of the control groups without H_2 (**Figure 8b~c**). For iC_5 and nC_5, the iC_5/nC_5 ratios are 1.27–2.25 (N = 5, Ave. = 1.67) and 0.72–1.01 (N = 5, Ave. = 0.84) under the catalytic action of $ZnCl_2$ and MoS_2, respectively. The value of iC_5/nC_5 under $ZnCl_2$ is about 1.98 times that under MoS_2, indicating that the change of iC_5 and nC_5 yield is affected more by Zn ion than Mo ion (**Figure 9A**). The iC_5/nC_5 ratio of H_2 reaction with $ZnCl_2$ and MoS_2 are 0.46–1.38 (N = 5, Ave. = 1.06) and 0.20–0.65 (N = 5, Ave. = 0.43), respectively (**Figure 9D**). The iC_5/nC_5 value under $ZnCl_2$ is about 2.47 times that under MoS_2. Meanwhile, the H_2 groups added by $ZnCl_2$ and MoS_2 are 0.63 and 0.51 of

the control groups iC_5/nC_5 without H_2, respectively (**Figure 9b~c**).

Therefore, the addition of exogenous H_2 changes the original pyrolysis evolution model of low-mature kerogen. As the C-C bond energy of gas component iC_m is greater than that of nC_m (Wang et al., 2011; Dai, 2014), it is easier to promote the generation of normal gaseous alkanes in the catalytic H_2 addition reaction, which preferentially promotes the increase of the yield of normal alkanes. In addition, the i/n ratio decreases significantly in the catalytic hydrogenation reaction. Meanwhile, the small molecule HC yield decreased significantly in the reaction catalyzed by H_2 addition of low-mature kerogen at a relatively low temperature.

4.3.2 FTT Synthesis May Occurduring Catalytic Hydrogenation Reaction

Large amounts of inorganic C_1 is formed through FTT synthesis reaction, and the estimated reaction temperatures can be less than 140°C in geologic settings (Young et al., 2017; Morrill et al., 2018; Etipe and Whiticar, 2019). The CO_2 yields are inhibited by the addition of exogenous H_2 during the reaction. For the gaseous HCs, the activation carbon source with low bond energy preferentially participates in the generation of long-chain carbon products with lower bond energy in the reaction stage at low temperature, resulting in the relatively insufficient generation of gaseous HCs with small molecular weight and affecting the pyrolysis and release of small molecular alkanes. At the high-temperature stage, the cracking degree of catalytic H_2 reaction is strengthened, resulting in a large increase in gaseous products. Decarboxylation is required in combination with Lewis acid catalytic mode. An important influencing factor of catalytic hydrogenation is determined by the abundance of oxygen-containing groups in the OM, which can promote more CO_2 production to participate in the FTT synthesis reaction. More gaseous HCs (mainly C_1) are generated, which has a certain increasing effect on the HCs. The decarboxylation corresponds to the HC increasing effect in OM mainly accompanied by Fischer-Tropsch synthesis contribution. In the kerogen reaction groups of Xiamaling Fm. (**Figure 3**), the change of CO_2 production is similar to that of the high-mature kerogen series (Huang et al., 2021), and the reduction range of CO_2 production decreases, which may be due to the high HI content of the formation increasing the alkane gas production. The yield of the hydrogenation groups does not increase significantly between 300°C and 500°C, revealing the consumption of CO_2 under FTT synthesis.

CONCLUSION

Catalytic hydrogenation plays an important role in the HC generation for the low-mature source rocks. Compared with the low-temperature state, the exogenous H_2 begins to participate in the catalytic pyrolysis reaction of kerogen in large quantities at the relatively high-temperature stage (≥400°C), promoting the increase of gaseous HC production. The maximum gaseous HC yield increases by about 3.2 times. The catalytic H_2 reaction significantly reduces the drying coefficient of natural gas at the relatively high-temperature stage and participates in FTT synthesis adding H_2 under the action of the catalyst. Through the comparison of the composition and isotope characteristics of gaseous products, the catalytic hydrogenation effect of $ZnCl_2$ on immature kerogen is better than MoS_2 under the same conditions, and mainly through cation action. It is revealed that exogenous H_2 and metal ions carried by the deep fluid have significant HC promotion effects on the yield of gaseous products under the catalytic hydrogenation condition.

DATA AVAILABILITY STATEMENT

The original contributions presented in the study are included in the article/Supplementary Material, further inquiries can be directed to the corresponding authors.

AUTHOR CONTRIBUTIONS

XH: Data curation, writing. ZJ: Conceptulization, writing. QL: Investigation, conceptulization. QM: Data curation, methodology. DZ: Methodology, investigation. LW: Investigation. JL: Methodology. PZ: Data curation. JW: Investigation.

FUNDING

This work was funded by National Key R&D Program of China (2019YFA0708504), National Natural Science Foundation of China (42172168, 41625009), and Strategic Priority Research Program of the Chinese Academy of Sciences (Class A) (XDA14010402 and XDA14010404).

ACKNOWLEDGMENTS

All the authors are grateful to Prof. Jinzhong Liu and Hong Lu for their experimental advice and sample assistance to support this study. We also thank. Dr. Qiang Wang and Yong Li for their laboratory help to improve the quality of the experimental results.

REFERENCES

Dai, J. (2014). *Natural Gas Geology and Geochemistry*, 6. Beijing: Petroleum Industry Press, 198–211.

Etiope, G. (2017). Abiotic Methane in Continental Serpentinization Sites: an Overview. *Procedia Earth Planet. Sci.* 17, 9–12. doi:10.1016/j.proeps.2016.12.006

Etiope, G., and Whiticar, M. J. (2019). Abiotic Methane in Continental Ultramafic Rock Systems: towards a Genetic Model. *Appl. Geochem.* 102, 139–152. doi:10.1016/j.apgeochem.2019.01.012

Guélard, J., Beaumont, V., Rouchon, V., Guyot, F., Pillot, D., Jézéquel, D., et al. (2017). Natural H2in Kansas: Deep or Shallow Origin? *Geochem. Geophys. Geosyst.* 18 (5), 1841–1865. doi:10.1002/2016gc006544

Guo, L. N., Ke, B. L., Liu, Q. J., Lin, H. L., Yin, T. Y., Lin, T. Y., et al. (2014). Shale Gas Organic Geochemistry Characteristic of the Mesoproterozoic Xiamaling Formation in Western Beijing Area. *Amr* 998-999, 1452–1457. doi:10.4028/www.scientific.net/amr.998-999.1452

He, K., Zhang, S., Mi, J., Chen, J., and Cheng, L. (2011). Mechanism of Catalytic Hydropyrolysis of Sedimentary Organic Matter with MoS2. *Pet. Sci.* 8 (02), 134–142. doi:10.1007/s12182-011-0126-0

Huang, X., Jin, Z., Liu, Q., Meng, Q., Liu, J., and Liu, J. (2021). Catalytic Hydrogenation of Post-mature Hydrocarbon Source Rocks under Deep-Derived Fluids: An Example of Early Cambrian Yurtus Formation, Tarim Basin, NW China. *Front. Earth Sci.* 9, 626111.

Jin, Z., Zhang, L., Yang, L., and Hu, W. (2004). A Preliminary Study of Mantle-Derived Fluids and Their Effects on Oil/gas Generation in Sedimentary Basins. *J. Pet. Sci. Eng.* 41 (1–3), 45–55. doi:10.1016/s0920-4105(03)00142-6

Jin, Z., Zhang, L., and Yang, L. (2002). Preliminary Study on Geochemical Characteristics of Fluids in Deep Sedimentary Basins and Hydrocarbon Accumulation Effect. *J. Earth Sci.* 27 (6), 659–665. doi:10.3321/j.issn:1000-2383.2002.06.001

Kissin, Y. V. (1987). Catagenesis and Composition of Petroleum: Origin of N-Alkanes and Isoalkanes in Petroleum Crudes. *Geochimica Cosmochimica Acta* 51 (9), 2445–2457. doi:10.1016/0016-7037(87)90296-1

Klein, F., Tarnas, J. D., and Bach, W. (2020). Abiotic Sources of Molecular Hydrogen on Earth. *Elements* 16 (1), 19–24. doi:10.2138/gselements.16.1.19

Liu, J., and Tang, Y. (1998). Kinetics of Early Methane Generation from Green River Shale. *Chin. Sci. Bull.* 43 (22), 1908–1912. doi:10.1007/bf02883470

Liu, Q., Dai, J., Jin, Z., Li, J., Wu, X., Meng, Q., et al. (2016). Abnormal Carbon and Hydrogen Isotopes of Alkane Gases from the Qingshen Gas Field, Songliao Basin, China, Suggesting Abiogenic Alkanes? *J. Asian Earth Sci.* 115, 285–297. doi:10.1016/j.jseaes.2015.10.005

Liu, Q., Zhu, D., Meng, Q., Liu, J., Wu, X., Zhou, B., et al. (2018). The Scientific Connotation of Oil and Gas Formations under Deep Fluids and Organic-Inorganic Interaction[J]. *Sci. China Earth Sci.* 62 (3), 507–528. doi:10.1007/s11430-018-9281-2

Lollar, B. S., Onstott, T. C., Lacrampe-Couloume, G., and Ballentine, C. J. (2014). The Contribution of the Precambrian Continental Lithosphere to Global H2 Production. *Nature* 516 (7531), 379–382. doi:10.1038/nature14017

Ma, X., Zheng, G., Sajjad, W., Xu, W., Fan, Q., Zheng, J., et al. (2018). Influence of Minerals and Iron on Natural Gases Generation during Pyrolysis of Type-III Kerogen. *Mar. Petroleum Geol.* 89, 216–224. doi:10.1016/j.marpetgeo.2017.01.012

Mango, F. D., and Hightower, J. (1997). The Catalytic Decomposition of Petroleum into Natural Gas. *Geochimica Cosmochimica Acta* 61 (24), 5347–5350. doi:10.1016/s0016-7037(97)00310-4

Mango, F. D. (1996). Transition Metal Catalysis in the Generation of Petroleum and Natural Gas. *Geochem. Cosmochim. Acta.* 56 (1), 553–555. doi:10.1016/0016-7037(92)90153-a

McCollom, T. M. (2016). Abiotic Methane Formation during Experimental Serpentinization of Olivine. *Proc. Natl. Acad. Sci. U.S.A.* 113 (49), 13965–13970. doi:10.1073/pnas.1611843113

Morrill, P., Cumming, E. A., Rietze, A., Morissey, L. S., Cook, M., Rhim, J. H., et al. (2018). *Sourcing Dissolved Methane from the Tablelands, Gros Morne National Park, NL, CAN: A Terrestrial Site of Serpentinization*. Boston: Goldschmidt Abstract 1816.

Qingqiang, M., Yuhua, S., Jianyu, T., Qi, F., Jun, Z., Dongya, Z., et al. (2015). Distribution and Geochemical Characteristics of Hydrogen in Natural Gas from the Jiyang Depression, Eastern China. *Acta Geol. Sin. - Engl. Ed.* 89 (5), 1616–1624. doi:10.1111/1755-6724.12568

Resing, J. A., Sedwick, P. N., German, C. R., Jenkins, W. J., Moffett, J. W., Sohst, B. M., et al. (2015). Basin-scale Transport of Hydrothermal Dissolved Metals across the South Pacific Ocean. *Nature* 523 (7559), 200–203. doi:10.1038/nature14577

Sun, X., Chen, J., Liu, W., and Zhang, S. (2003). Hydrothermal Venting on the Seafloor and Formation of Organic-Rich Sediments-Eevidence from the Neoproterozoic Xiamaling Formation, North China. *Geol. Rev.* 49 (6), 588–595.

Tivey, M. (2007). Generation of Seafloor Hydrothermal Vent Fluids and Associated Mineral Deposits. *Oceanogr* 20 (1), 50–65. doi:10.5670/oceanog.2007.80

Wang, Q., Jia, W., Yu, C., Song, J., Zhang, H., Liu, J., et al. (2020). Potential of Light Oil and Condensates from Deep Source Rocks Revealed by the Pyrolysis of Type I/II Kerogens after Oil Generation and Expulsion. *Energy fuels.* 34 (8), 9262–9274. doi:10.1021/acs.energyfuels.0c00553

Wang, X., Liu, W., Xu, Y., and Zheng, J. (2011). Influences of Water Media on the Hydrogen Isotopic Composition of Natural Gas/methane in the Processes of Gaseous Hydrocarbon Generation and Evolution. *Sci. China Earth Sci.* 54 (9), 1318–1325. doi:10.1007/s11430-011-4195-0

Xie, L., Sun, Y., Yang, Z., Chen, J., Jiang, A., Zhang, Y., et al. (2013). Evaluation of Hydrocarbon Generation of the Xiamaling Formation Shale in Zhangjiakou and its Significance to the Petroleum Geology in North China. *Sci. China Earth Sci.* 56, 444–452. doi:10.1007/s11430-012-4538-5

Young, E. D., Kohl, I. E., Lollar, B. S., Etiope, G., Rumble, D., III, Li, S., et al. (2017). The Relative Abundances of Resolved l2CH2D2 and 13CH3D and Mechanisms Controlling Isotopic Bond Ordering in Abiotic and Biotic Methane Gases. *Geochimica Cosmochimica Acta* 203, 235–264. doi:10.1016/j.gca.2016.12.041

Zhang, S., Zhang, B., Bian, L., Jin, Z., Wang, D., and Chen, J. (2007). The Xiamaling Oil Shale Generated through Rhodophyta over 800 Ma Ago. *Sci. China Ser. D.* 50, 527–535. doi:10.1007/s11430-007-0012-1

Conflict of Interest: The authors declare that the research was conducted in the absence of any commercial or financial relationships that could be construed as a potential conflict of interest.

Publisher's Note: All claims expressed in this article are solely those of the authors and do not necessarily represent those of their affiliated organizations, or those of the publisher, the editors and the reviewers. Any product that may be evaluated in this article, or claim that may be made by its manufacturer, is not guaranteed or endorsed by the publisher.